Journal of Photochemistry and Photobiology A: Chemistry 216 (2010) 275–282

Contents lists available at ScienceDirect

Journal of Photochemistry and Photobiology A: Chemistry

journal homepage: www.elsevier.com/locate/jphotochem

Preparation of Fe-modified photocatalysts and their application for generation of useful hydrocarbons during photocatalytic decomposition of acetic acid

Sylwia Mozia*, Aleksandra Heciak, Antoni W. Morawski

West Pomeranian University of Technology, Institute of Chemical and Environment Engineering, ul. Pułaskiego 10, 70-322 Szczecin, Poland

ARTICLE INFO

Article history:
Available online 29 September 2010

Keywords:
Photocatalysis
Hydrocarbons
Methane
Acetic acid
Fe/TiO_2

ABSTRACT

The present study was focused on the photocatalytic generation of useful hydrocarbons and hydrogen from acetic acid under N_2 atmosphere. The photocatalysts applied in the study were prepared from a crude TiO_2 modified with $Fe(CH_3COO)_2$ and calcinated at the temperatures of 400, 500 or 600 °C in argon atmosphere. In order to compare the results, the commercially available photocatalyst AEROXIDE® P25 (Evonik, former Degussa, Germany) was also used in the experiments. The photocatalysts were characterized by UV–vis/DR and FTIR spectroscopy, N_2 adsorption–desorption at 77 K and XRD measurements. The crystallite size of anatase was in the range of 7–28 nm and the anatase over rutile ratio was from 82:18 to 95:5. The main gaseous products of CH_3COOH decomposition were CH_4 and CO_2. Moreover, ethane, propane and hydrogen were detected in the gaseous reaction mixtures. The most active photocatalyst towards CH_4 generation was TiO_2 containing 20 wt.% of Fe calcinated at 500 °C. After 27 h of the process conducted with this catalyst the amount of CH_4, CO_2, C_2H_6, C_3H_8 and H_2 evolved was 3.36, 2.97, 0.13, 0.01 and 0.14 mmol/mol CH_3COOH, respectively. It was concluded that photocatalytic decomposition of organic compounds, such as acetic acid, under N_2 atmosphere could be regarded as a method of production of environmentally friendly "photo-biogas"; however, since the yield of hydrocarbons formation was very low, deep and extensive investigations are still necessary in order to improve the efficiency of the process.

1. Introduction

Progressively decreasing resources of fossil fuels as well as the global warming problem have recently resulted in the development of new alternative methods of energy production. Taking into consideration that another global problem is pollution of the environment, it would be desirable to link both, waste or wastewater treatment and their conversion into useful energy [1–3]. One solution for that could be biogas production.

A promising alternative to the traditional method of biogas production which is anaerobic digestion seems to be generation of methane and other useful hydrocarbons via photocatalytic reactions. Since photocatalysis, in general, is not specific for particular substrates, it could be applied for any types of contaminants, even those, which are toxic to bacteria [4]. This enhances the competitiveness of photocatalysis in the discussed application.

The most often applied photocatalyst, due to its significant activity, high stability and low cost, is TiO_2. A majority of the already published papers [5–10] describing the photocatalytic production of methane concern a reduction of CO_2 under UV light in the presence of pure or modified TiO_2. For example, Tan et al. [6,7] presented their experimental study on the photocatalytic reduction of CO_2 in the presence of H_2O using TiO_2 pellets illuminated with UV light. The authors found that during the process low amounts of H_2 and CO were produced except from methane. When UVC (253.7 nm) light was used, the total yield of methane was approximately 200 ppm. Switching from UVC to UVA (365 nm) resulted in a significant decrease in the yield of CH_4 generation [7].

The literature data concerning photocatalytic generation of methane from organic compounds in liquid phase are very limited. All of them describe production of CH_4 from aliphatic acids [11–14] and alcohols [15]. In 1970s Kraeutler and Bard [11–13] published a series of papers reporting photocatalytic decarboxylation of acetic acid in the presence of Pt/TiO_2 catalyst. The main products of the reaction were methane and carbon dioxide. Similarly, Sakata et al. [14] observed methane and ethane formation during photodecomposition of acetic and propionic acids in the presence of TiO_2 and Pt/TiO_2.

A development of an effective photocatalyst is one of the most important aspects in the photocatalytic generation of methane. The already published papers focus on the application of either TiO_2 or Pt/TiO_2 photocatalysts [11–15]. To our best knowledge, no attempts to utilize Fe-modified TiO_2 in this process have been undertaken till now. During the present research different TiO_2

* Corresponding author. Tel.: +48 91 449 47 30; fax: +48 91 449 46 86.
E-mail address: sylwia.mozia@zut.edu.pl (S. Mozia).

1010-6030/$ – see front matter © 2010 Elsevier B.V. All rights reserved.
doi:10.1016/j.jphotochem.2010.09.016

powders modified with Fe compounds were applied for photocatalytic generation of useful hydrocarbons, mainly methane, under N_2 atmosphere. Moreover, the effectiveness of H_2 formation was also determined. The influence of catalyst properties on the reaction yield was especially investigated. Fe was selected on a basis of literature data concerning degradation of organic compounds [16,17] and hydrogen production [18]. Papers show that Fe, in a proper concentration, can increase the photoactivity of TiO_2 photocatalysts. In the literature data it can be found that the amount of Fe incorporated in a photocatalyst could be as low as 0.05 at.% [16] or as high as 50 at.% [21]. In general, Fe-modified TiO_2 could be divided into two main groups: (1) low-loaded (or doped) photocatalysts [16–20] and (2) high-loaded (or composite) photocatalysts [19,21–23]. Zhu et al. [22] reported that at low Fe doping concentrations ($\leq$2 wt.%), Fe atoms substitute for the sites of Ti atoms in the anatase lattice, whereas at higher Fe concentrations iron exist in two forms: some Fe ions are incorporated into the anatase lattice, while others aggregate to Fe_2O_3 or Fe_3O_4.

During the present research we have focused on high-loaded photocatalysts, which, in general, are much less investigated than the Fe-doped TiO_2. An important advantage of the Fe-modified TiO_2 with high iron content is high stability of these catalysts, in terms of photocorrosion, compared to Fe-doped titania, as reported by Litter and Navío [19]. Moreover, photocatalytic activity of heavily loaded Fe/TiO_2 samples has been proved [21].

Acetic acid was used as a source of "photo-biogas". The main reason for studying decomposition of this compound was that it undergoes the "photo-Kolbe" reaction in which methane and carbon dioxide, being the main components of the conventional biogas, are formed. Moreover, an application of acetic acid as a model compound seems to be reasonable since amongst the final by-products of photocatalytic degradation of most organic compounds in water different aliphatic acids, including CH_3COOH, are present.

2. Experimental

2.1. Photocatalysts

The photocatalysts used in this study were prepared from crude TiO_2 obtained directly from the production line (sulphate technology) at the Chemical Factory "Police" (Poland). The crude TiO_2 was modified with $Fe(CH_3COO)_2$ as follows. A defined amount of TiO_2 was introduced into a beaker containing aqueous solution of $Fe(CH_3COO)_2$ and stirred for 22 h. After that water was evaporated and the samples were dried at 80 °C for 24 h in an oven. Such prepared samples were calcinated at 400, 500 or 600 °C in Ar atmosphere for 1 h (83 dm^3/min). The amount of Fe introduced to the samples was 10, 20 or 30 wt.%. The samples modified with $Fe(CH_3COO)_2$ were denoted as A-Fe*X*Ac*Y* (A-Fe10Ac400, A-Fe10Ac500, A-Fe10Ac600, A-Fe20Ac500 and A-Fe30Ac500), where *X* refers to Fe content (10–30 wt.%) and *Y* to the calcination temperature (400–600 °C). In order to compare the results crude TiO_2 without $Fe(CH_3COO)_2$ was calcinated at 500 °C for 1 h (A500). Moreover, the commercially available photocatalyst AEROXIDE® P25 (Evonik, formerly Degussa, Germany) and Fe_3O_4 nanopowder (<50 nm, $\geq$98%; Aldrich) were also applied in the photocatalytic experiments.

2.2. Characterization of the photocatalysts

The XRD patterns were recorded using X'Pert PRO diffractometer with Cu Kα radiation (λ = 1.54056 Å). TiO_2 anatase over rutile ratio was calculated from [24]:

$$\text{anatase content } A = \frac{1}{1 + 1.26(I_R/I_A)} \quad (1)$$

where I_A and I_R are the diffraction intensities of the (1 0 1) anatase and (1 1 0) rutile crystalline phases at 2θ = 25.3° and 27.4°, respectively. The average anatase crystallite diameter D (nm) was calculated using Scherrer's equation [24,25]:

$$D = \frac{K\lambda}{\beta \cos\theta} \quad (2)$$

where K = 0.9 is a shape factor for spherical particles, λ is the wavelength of the incident radiation (λ = 1.54056 Å), θ is half of the diffraction angle (rad) and β is the line width at half-maximum height. The phase identification was conducted by comparing the measured patterns against the JCPDS cards from the powder diffraction file database published by the Joint Committee on Powder Diffraction Standards.

The FTIR spectra were recorded using Jasco FT-IR 430 spectrometer (Japan) equipped with a diffuse reflectance accessory (Harrick, USA).

The UV–vis/DR spectra were recorded using Jasco V 530 spectrometer (Japan) equipped with an integrating sphere accessory for diffuse reflectance spectra. $BaSO_4$ was used as a reference.

The Brunauer–Emmett–Teller (BET) surface area of the powders was determined on the basis of nitrogen adsorption–desorption measurements at 77 K conducted in Quadrasorb SI (Quantachrome, USA) apparatus. All of the samples were degassed at 80 °C prior to nitrogen adsorption measurements. The BET surface area was determined by multipoint BET method using the adsorption data.

2.3. Photocatalytic reaction

The photocatalytic reaction was conducted in a cylindrical glass reactor (Heraeus, type UV-RS-2) equipped with a medium pressure mercury vapour lamp (TQ-150, λ_{max} = 365 nm). The total volume of the reactor was 765 cm^3. In the upper part of the reactor a gas sampling port was located. At the beginning of the experiment 0.35 dm^3 of CH_3COOH solution (1 mol/dm^3) and 0.35 g of a catalyst were introduced into the reactor. Thus, the headspace volume in the reactor was equal to 415 cm^3. Before the photocatalytic reaction N_2 was bubbled through the reactor for at least 1 h to ensure that the dissolved oxygen was eliminated. Then, the N_2 flow was stopped and UV lamp, positioned in the centre of the reactor, was turned on to start the photoreaction. The process was conducted for 27 h. The reaction mixture containing photocatalyst in suspension was continuously stirred during the experiment by means of a magnetic stirrer.

All the experiments were repeated at least twice in order to confirm the reproducibility of the results. The presented data are mean values obtained from the two experiments (S.D. were below 9%).

Gaseous products of the reaction were analyzed using GC SRI 8610C equipped with TCD and HID detectors, and Shincarbon (carbon molecular sieve; 2 m, 1 mm, 100–120 mesh) and molecular sieve 5A (3 m, 2 mm, 80–100 mesh) or 13× (1.8 m, 2 mm, 80–100 mesh) columns. Helium was used as the carrier gas. The composition of the liquid phase was determined using GC SRI 8610C equipped with FID detector and MXT®-1301 (60 m) column. Hydrogen was used as the carrier gas.

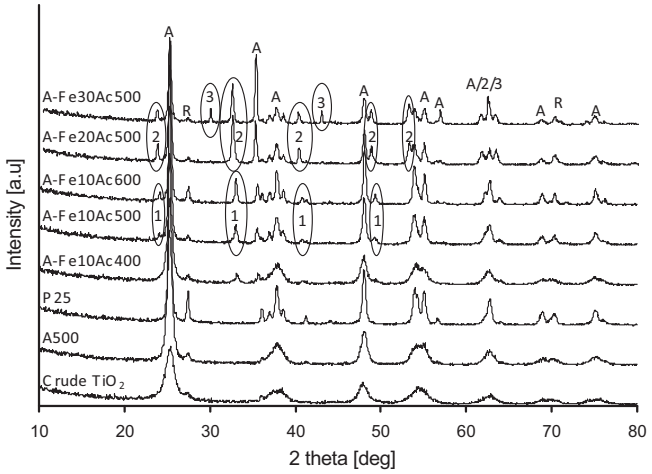

Fig. 1. XRD patterns of photocatalysts: (A) anatase; (R) rutile; (1) $Fe_{1.66}Ti_{0.34}O_3$; (2) $FeTiO_3$; (3) Fe_3O_4.

3. Results and discussion

3.1. Physico-chemical properties of the photocatalysts

Fig. 1 shows the XRD patterns of the TiO_2 and Fe/TiO_2 photocatalysts. The phase composition of the photocatalysts is presented in Table 1. It can be observed that crude TiO_2 contained anatase and rutile phases in the ratio of 85:15. The diffraction lines were weak and broad suggesting poor crystallinity of the sample. The crystallite size of anatase in the crude TiO_2 was 7 nm. The heat treatment of crude TiO_2 (A500) resulted in an improvement of TiO_2 crystallinity associated with anatase crystals growth (12 nm vs. 7 nm, Table 1). In case of the sample modified with $Fe(CH_3COO)_2$ the crystallite size of anatase was in the range of 12–28 nm. It was also found that the heat treatment of Fe/TiO_2 resulted in sharpening and narrowing of diffraction lines (Fig. 1). The thermal treatment significantly affected the crystallite size of anatase, which was increasing with increasing calcination temperature. This indicates aggregation of TiO_2 nanoparticles upon annealing. The samples A500 and A-Fe10Ac500 annealed at the same temperature of 500 °C have different crystallinity (12 nm vs. 21 nm). These results indicate that Fe catalyzes a growth of crystallites of anatase upon annealing [25]. Moreover, the obtained data suggest that the properties of the products obtained during modification of TiO_2 with iron compounds strongly depend on the concentration of Fe introduced into the samples and temperature of calcination.

According to Litter and Navió [19] TiO_2 particles can be simply substitutionally doped by iron, the photocatalysts can be mixtures of TiO_2 with iron oxide, or coexisting mixed oxides can be present. Since the Fe^{3+} radius (0.64 Å) is similar to that of Ti^{4+} (0.68 Å) [26] the substitution of iron in the matrix is an easy process. During calcination, the preadsorbed precursor is decomposed, and iron initially present at the surface diffuses into the bulk producing a solid solution. Specimens containing less Fe are substitutional solid solutions in which iron ions are dispersed in the lattice of TiO_2. Specimens containing higher iron contents accommodate any excess of iron as minute particles or small aggregates of iron oxide and/or mixed oxides of Fe and Ti at the surface of the solid solution particles. Some intermediate states could be present, depending on the transformation of anatase to rutile and on the solubility limit of iron in both phases [19]. Detailed analysis of the XRD patterns of our photocatalysts revealed that in case of the samples containing 10 wt.% of Fe such intermediate state is present (Fig. 1). It was identified as $Fe_{1.66}Ti_{0.34}O_3$. The composition of this mixed oxide was calculated from a correlation curve representing the dependence of the lattice constant (d) on Ti fraction in the oxide. During the calculations the following JCPDS cards were applied: 01-089-0599, 04-009-5898, 04-006-6608, 01-0708156, 01-070-8179, 04-006-6576, 04-006-6577, 01-073-1256, 01-073-1255, 01-075-1207. In case of the samples containing 20 and 30 wt.% of Fe both, iron oxide (Fe_3O_4) and mixed oxide – ilmenite ($FeTiO_3$) were identified. The presence of these species suggests that Fe^{2+} from $Fe(CH_3COO)_2$ was only partially oxidized to Fe^{3+}. Fe_3O_4 and $FeTiO_3$ were identified by comparison of the measured XRD patterns with the JCPDS cards (Nos. 01-089-0599 and 01-071-6766).

Fig. 2a shows FTIR spectra of the crude, annealed and Fe-modified TiO_2. It can be seen that the intensity of the bands associated with –OH vibrations (3300–3500 cm^{-1}) decreased with increasing the heat treatment temperature. This indicates that the amount of hydroxyl groups present on TiO_2 surface was reduced upon annealing, especially in case of Fe/TiO_2. These data suggest that the presence of Fe ions changes the content of surface –OH groups [19]. The bands observed at 1630–1640 cm^{-1} can be assigned to molecular water bending mode [27]. Pure titania (P25, A500, crude TiO_2) and A-Fe10Ac400 spectra exhibit, in the ν(OH) region, one band with a maximum at 3685–3700 cm^{-1}, which characterizes the stretching vibrations of Ti^{4+}–OH surface hydroxyl groups. In the low frequency region (below 1000 cm^{-1}) the self-absorption of titania [21] is observed, which is especially strong in case of pure TiO_2 and the samples with low Fe content. Moreover, in the spectra of TiO_2 containing 20 and 30 wt.% of Fe (Fig. 2b) the absorption bands between 600 and 750 cm^{-1} can be seen. The intensity of these bands is stronger in case of the photocatalyst with higher iron content (A-Fe30Ac500) than in case of A-Fe20Ac500. The observed absorption in the 600–750 cm^{-1} region could be associated with the presence of iron in the catalysts structure. This supposition could be confirmed by a comparison of the spectra of the Fe-modified TiO_2 with the spectra of Fe_3O_4 and TiO_2 (A500). In the spectrum of pure titania no bands between 600 and 750 cm^{-1} are present, whereas the spectrum of Fe_3O_4 exhibits a distinct increase of absorbance in this region.

Fig. 3 shows UV–vis/DR spectra of the TiO_2 and Fe/TiO_2 powders containing different Fe concentration and calcinated at different temperatures. In general, the light absorption characteristic of TiO_2 is affected by the presence of metal ions [16]. A significant increase in the absorption at wavelengths longer than 400 nm was observed for the Fe-modified samples (Fig. 3). The spectra of these

Table 1
Physico-chemical properties of the photocatalysts: (A) anatase; (R) rutile.

Sample	Specific surface area, S_{BET} [m^2/g]	Phase composition by XRD	Crystallite size of anatase [nm]	Anatase over rutile ratio (A:R)
Crude TiO_2	215	A, R	7	85:15
A500	103	A, R	12	92:8
P25	50	A, R	22	82:18
A-Fe10Ac400	82	A, R, $Fe_{1.66}Ti_{0.34}O_3$	12	90:10
A-Fe10Ac500	34	A, R, $Fe_{1.66}Ti_{0.34}O_3$	21	93:7
A-Fe10Ac600	18	A, R, $Fe_{1.66}Ti_{0.34}O_3$	28	90:10
A-Fe20Ac500	19	A, R, $FeTiO_3$	24	95:5
A-Fe30Ac500	19	A, R, $FeTiO_3$, Fe_3O_4	24	95:5

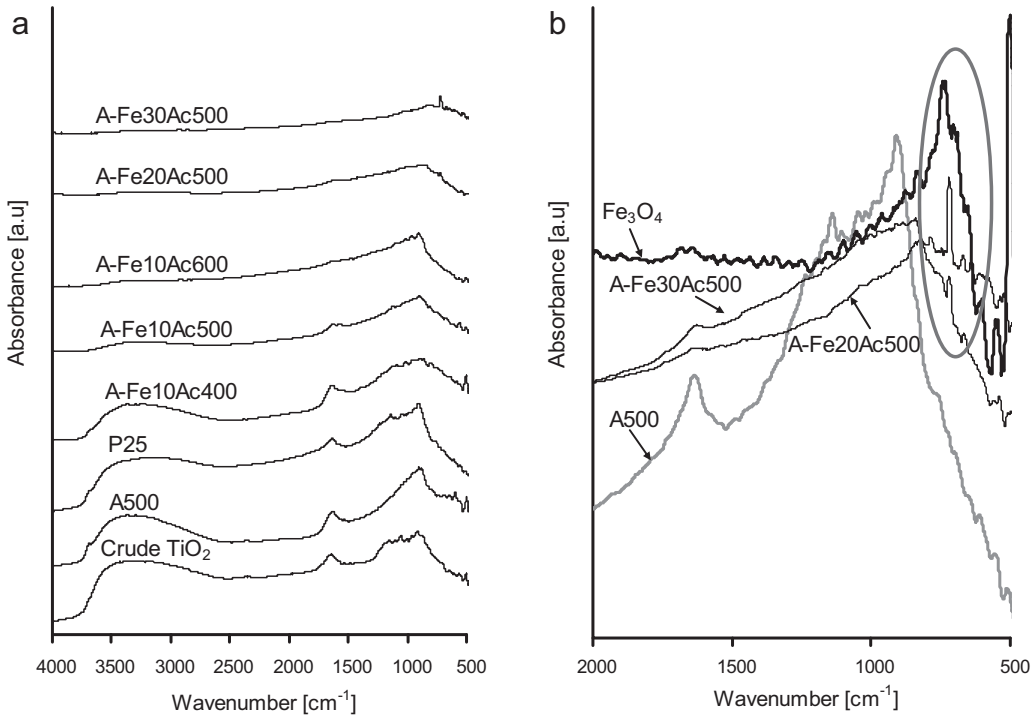

Fig. 2. FTIR spectra of photocatalysts and Fe_3O_4.

photocatalysts show a strong absorption in the visible light region and are red shifted compared to the spectra of pure titania. Red shift associated with the presence of Fe ions could be attributed to a charge transfer transition between Fe ions electrons and TiO_2 conduction or valence bands [28]. With increasing Fe concentration the samples show a stronger absorption in the visible range which might be attributed to a dark color of the powders. The observed absorption in the vis region might indicate that TiO_2 samples modified with Fe could be active under visible light [29].

The specific BET surface area (S_{BET}) of the photocatalysts is presented in Table 1. It can be seen that the surface area of the pure titania samples decreased with increasing calcination temperature from 215 m^2/g in case of crude TiO_2 to 103 m^2/g for A500. In case of the Fe-modified TiO_2, the BET surface area decreased with the annealing temperature from 82 m^2/g for A-Fe10Ac400 to 18 m^2/g for A-Fe10Ac600. Moreover, it could be observed that the S_{BET} of the Fe-modified photocatalysts calcinated at 500 °C was 3–5 times lower than the S_{BET} of A500. These results clearly show that the presence of Fe compounds strongly affects the surface area of the photocatalysts [21]. A decrease of S_{BET} might be also attributed to larger crystallite size of anatase in the Fe/TiO_2 compared to pure titania A500 (Table 1).

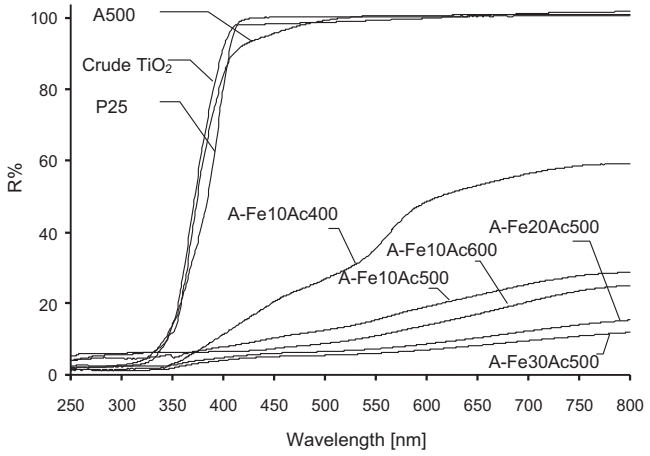

Fig. 3. UV–vis/DR spectra of different photocatalysts.

3.2. Photocatalytic decomposition of acetic acid

The commercially available P25, crude and annealed TiO_2 as well as the Fe modified TiO_2 photocatalysts were applied in the photocatalytic decomposition of acetic acid under N_2 atmosphere. The reaction was conducted for 27 h. Regardless of the photocatalyst used the gaseous products identified during the photocatalytic decomposition of CH_3COOH were CH_4, CO_2, C_2H_6, C_3H_8 and H_2. The concentrations of these compounds in the gaseous phase (headspace volume of the reactor) were dependent on the photocatalyst applied. Nevertheless, in all the experiments CH_4 and CO_2 were obtained at the highest amounts.

3.2.1. Hydrocarbons production from acetic acid

The principal purpose of this study was to investigate the photocatalytic generation of hydrocarbons, mainly methane, in the presence of different photocatalyst. The obtained results are presented in Figs. 4 and 5.

Methane formation during photocatalytic decomposition of acetic acid follows the so-called photo-Kolbe reaction pathway. The products of this reaction are methane and carbon dioxide [11–14]:

$$CH_3COOH \rightarrow CH_4 + CO_2 \quad (3)$$

Reaction (3) represents the photocatalytic decarboxylation of acetic acid. The reaction is initiated by photogenerated holes and can be also written as follows [14]:

$$CH_3COOH + h^+ \rightarrow CH_3^{\bullet} + CO_2 + H^+ \quad (4)$$

$$H + e^- \rightarrow H^{\bullet} \quad (5)$$

$$CH_3^{\bullet} + H^{\bullet} \rightarrow CH_4 \quad (6)$$

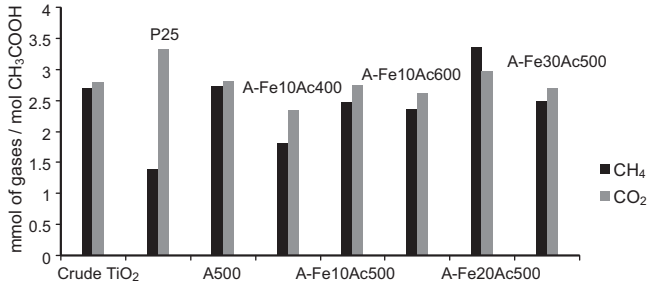

Fig. 4. Comparison of the amounts of CH_4 and CO_2 evolved after 27 h of irradiation in the presence of different photocatalysts.

The reaction of the formation of ethane from acetic acid can be presented as follows [14]:

$$CH_3COOH \rightarrow C_2H_6 + 2CO_2 + H_2 \quad (7)$$

or, taking into consideration the recombination of methyl radicals [10]:

$$CH_3^{\bullet} + CH_3^{\bullet} \rightarrow C_2H_6 \quad (8)$$

In the same way the reaction of the formation of propane could be written as:

$$3CH_3COOH \rightarrow C_3H_8 + 3CO_2 + 2H_2 \quad (9)$$

Fig. 4 shows the amounts of methane and carbon dioxide evolved after 27 h of irradiation. It was found that the amounts of both gases continuously increased during the process. After the initial 5 h of the reaction the amount of CH_4 was in the range of 0.33–0.88 mmol/mol CH_3COOH. The highest yield of methane evolution was observed for A-Fe20Ac500 and the lowest for P25 photocatalysts. In case of CO_2, the amount of this product in the gaseous phase after 5 h of irradiation ranged from 0.52 to 0.98 mmol/mol CH_3COOH. The lowest amount of carbon dioxide was produced in case of A500. The highest yield of CO_2 evolution was observed in the presence of P25 catalyst. Elongation of the reaction time resulted in further increase of the concentrations of both gases. After 27 h of irradiation the amount of CH_4 was in the range of 1.39–3.36 mmol/mol CH_3COOH being the highest for A-Fe20Ac500 (Fig. 4). The amount of CO_2 at the end of the process ranged from 2.34 to 3.32 mmol/mol CH_3COOH. The lowest concentration of CO_2 was observed in case of A-Fe10Ac500, whereas the highest was found in case of P25.

As was mentioned earlier, amongst the gaseous products of the reaction ethane and propane were also identified. The amounts of these gaseous compounds evolved in the presence of different photocatalysts are shown in Fig. 5. In general, the amounts of C_2H_6 and C_3H_8 were significantly lower compared to those of CH_4 and CO_2.

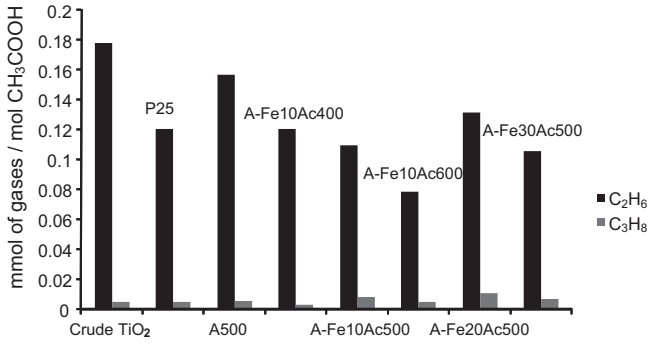

Fig. 5. Comparison of the amounts of C_2H_6 and C_3H_8 evolved after 27 h of irradiation in the presence of different photocatalysts.

The amount of C_2H_6 after 5 h of the irradiation was in the range of 0.03–0.06 mmol/mol CH_3COOH. The amount of ethane after 27 h of irradiation ranged from 0.08 to 0.18 mmol/mol CH_3COOH. The highest yield of ethane evolution was observed for crude TiO_2, A500 and A-Fe20Ac500, whereas the lowest for A-Fe10Ac600. At the end of irradiation the amount of C_3H_8 was found to be in the range of 0.003–0.010 mmol/mol CH_3COOH. The highest effectiveness of propane generation was observed in case of A-Fe20Ac500, and the lowest in case of A-Fe10Ac400.

The presented data show that the transformation efficiency of CH_3COOH to CH_4 determined after 27 h of irradiation was about 0.14–0.34%, depending on the photocatalyst. One might regard it as a drawback of this process. However, it should be noticed that the concentration of acetic acid at the beginning of the experiment was 1 mol/dm^3, which is very high. Therefore, the time necessary for a complete decomposition of CH_3COOH is very long. The process was conducted for 27 h only. Taking into consideration that the concentration of CH_4 was continuously increasing in time, it could be supposed that the transformation efficiency at longer times would be higher. However, in order to state it unequivocally, further investigations are necessary.

The yields of ethane and propane evolution were significantly lower than that of methane which clearly indicates that the reactions (7) and (9) are of minor importance.

From the reaction (3) it could be found that every one mole of acetic acids gives one mole of methane and one mole of carbon dioxide, i.e. the CH_4/CO_2 ratio should be equal to 1. However, in the performed experiments the CH_4/CO_2 ratio differed from unity. The CH_4/CO_2 ratio calculated after 27 h of irradiation was equal to 0.96, 0.97 and 0.42 for crude TiO_2, A500 and P25 respectively, and 0.78, 0.91, 0.91, 1.13, 0.92 for A-Fe10Ac400, A-Fe10Ac500, A-Fe10Ac600, A-Fe20Ac500 and A-Fe30Ac500, respectively. Due to the fact that solubility of carbon dioxide in water, although limited, is still about one order of magnitude higher compared to that of methane, one might expect that concentration of CO_2 in the gaseous phase should be lower than that of CH_4. Such a situation was observed only in case of Fe/TiO_2 with 20 wt.% of Fe (A-Fe20Ac500). However, in case of all other samples the amount of CO_2 evolved from the solution was higher than that of methane. This might suggest that except from the photo-Kolbe reaction (3) some other reactions in which CO_2 is produced proceed in the system. Carbon dioxide is also generated in the reactions (7) and (9). However, taking into consideration that the amounts of ethane and propane were very low, it is rather doubtful that such a high concentration of CO_2 as one observed in case of P25 was produced in these reactions.

The formation of higher amount of CO_2 than CH_4 during photocatalytic decomposition of acetic acid was already reported in the literature [14,30–32]. These reports were published during the last 30 years, nevertheless, none of them explicate that phenomenon unequivocally. Sakata et al. [14] concluded that the CO_2/CH_4 ratio greater than unity suggested that the oxidation of organic acids proceeded further, but no mechanism for that was proposed. Yoneyama et al. [30] argued that a high concentration of CO_2 might result from decomposition of organic intermediates, like ethanol or acetaldehyde to CO_2 and H_2. However, in their investigations a significant yield of hydrogen formation was observed, a phenomenon that did not take place in our system (see Section 3.2.2). The authors [30] also postulated a formation of hydroxyl radicals in competition with methyl radicals and their involvement in the subsequent reactions to yield finally CO_2 as the main product. On the basis of the results obtained during our investigations (Fig. 4), we suggest that the excess of carbon dioxide originated from the mineralization of acetic acid to H_2O and CO_2. Very high photocatalytic activity of the commercial P25 in degradation and mineralization of organic compounds is well known and widely described in numerous publications. This high photoactivity is

associated mainly with efficient formation of hydroxyl radicals, being the main oxidizing agents during photocatalytic reactions. However, direct oxidation of acetic acid with •OH does not result in the formation of CO_2 and H_2O [30]:

$$CH_3COOH + OH^\bullet \rightarrow CH_3^\bullet + CO_2 + H_2O \quad (10)$$

The mineralization of acetic acid to CO_2 and H_2O could take place in the presence of oxygen:

$$CH_3COOH + 2O_2 \rightarrow 2CO_2 + 2H_2O \quad (11)$$

Since atmospheric oxygen was not present in the system, the involvement of photogenerated O_2 should be considered [33,34]:

$$OH^\bullet + OH^\bullet \rightarrow H_2O_2 \quad (12)$$

$$H_2O_2 + 2h^+ \rightarrow O_2 + 2H^+ \quad (13)$$

$$H_2O_2 + OH^\bullet \rightarrow H_2O + HO_2^\bullet \quad (14)$$

$$HO_2^\bullet + OH^\bullet \rightarrow H_2O + O_2 \quad (15)$$

$$HO_2^\bullet + H^+ + e^- \rightarrow H_2O_2 \quad (16)$$

$$2H_2O_2 \rightarrow 2H_2O + O_2 \quad (17)$$

The reaction of photogenerated oxygen with acetic acid could subsequently lead to mineralization of CH_3COOH according to Eq. (11).

It could not be excluded that mineralization of CH_3COOH took place not only in the presence of P25 but also in case of other photocatalysts. However, since the CH_4/CO_2 ratio obtained with these samples was close to 1 it could be supposed that the photo-Kolbe reaction pathway was the primary one in case of these catalysts.

In order to clarify the reaction mechanism it is important to identify the products in the aqueous medium besides those in the gaseous phase. The compounds detected in the liquid phase during photocatalytic decomposition of acetic acid were methanol (CH_3OH), ethanol (C_2H_5OH), acetone ($CO(CH_3)_2$), acetaldehyde (CH_3CHO) and methyl acetate (CH_3COOCH_3).

The concentrations of these products were very low and did not exceed 10 μmol/dm^3. •OH radicals are known to have a strong oxidation power and can easily oxidize various organic compounds. The presence of the reaction products in liquid phase is explained reasonably by assuming an involvement of these radicals [14]:

$$CH_3^\bullet + OH^\bullet \rightarrow CH_3OH \quad (18)$$

$$CH_3OH + CH_3COOH \rightarrow CH_3COOH_3 + H_2O \quad (19)$$

$$C_2H_5^\bullet + OH^\bullet \rightarrow C_2H_5OH \quad (20)$$

$$C_2H_5OH + 2OH^\bullet \rightarrow CH_3CHO + 2H_2O \quad (21)$$

Some of the organic intermediates, e.g. methanol might be further decomposed to form CO_2 and H_2 [14]:

$$CH_3OH + H_2O \rightarrow CO_2 + 3H_2 \quad (22)$$

Moreover, other compounds obtained during acetic acid decomposition, such as acetaldehyde might undergo mineralization yielding CO_2 as the product [35,36]. Liu et al. [35] proposed the following mechanism of acetaldehyde mineralization when the number of the holes photogenerated on TiO_2 surface is much larger than the number of the adsorbed acetaldehyde molecules:

$$CH_3CHO + 3H_2O + 10h^+ \rightarrow 2CO_2 + 10H^+ \quad (23)$$

Taking into consideration Eqs. (10)–(23) it could be concluded that in the presence of hydroxyl radicals or photogenerated oxygen numerous reactions might occur in the system investigated, including mineralization of acetic acid or formation of organic intermediates in the liquid phase and their further decomposition. These reactions might yield CO_2 as the main product, which could explicate why the CH_4/CO_2 ratio differs from unity in case of some TiO_2 samples.

On the basis of the results obtained at the end of irradiation the activity of the photocatalysts towards methane generation can be put in the following order: A-Fe20Ac500 > crude TiO_2 ≈ A500 > A-Fe30Ac500 > A-Fe10Ac500 > A-Fe10Ac600 > A-Fe10Ac400 > P25. Comparing these data with the specific BET surface area of the photocatalysts (Table 1) it could be concluded that S_{BET} did not influence the activity of photocatalysts towards CH_4 formation. For example, P25, having about 2.5 times higher BET surface area than A-Fe20Ac500 (50 m^2/g vs. 19 m^2/g) exhibited lower activity in CH_4 generation than the sample containing 20 wt.% Fe calcinated at 500 °C. The highest surface area exhibited crude TiO_2 (215 m^2/g); however, it was less effective than A-Fe20Ac500. These results suggest that some other parameters were responsible for the activity of TiO_2 in the photo-Kolbe reaction. Such parameters could be phase composition, crystallinity and the presence of iron ions in the samples.

It was observed that A-Fe10Ac400, A-Fe10Ac600 and P25, characterized by the highest rutile content from all the catalysts (Table 1), were the least effective in CH_4 production. In general, rutile is considered a poor photocatalyst. Low photocatalytic activity of rutile in photodegradation of organic compounds is usually attributed to high recombination rate of photogenerated electrons and holes or changes in the specific surface area and porosity [37]. Higher activity of A-Fe20Ac500 compared to other catalysts calcinated at the same temperature (A500, A-Fe10Ac500) could be associated with the crystal size of anatase in this sample (Table 1). The XRD patterns show sharp and narrow diffraction lines in case of A-Fe20Ac500. This corresponded to the improvement of TiO_2 crystallinity associated with anatase crystals growth (24 nm vs. 12 and 21 nm). Moreover, the A-Fe20Ac500 catalyst contained a very low amount of rutile (A:R ratio equal to 95:5, Table 1), which might also contribute to its activity.

Somehow, Fe must play an important role during the photocatalytic reaction. Hung et al. [17] proposed that the improved activity of Fe/TiO_2 is due to either one or a combination of the following factors: (a) increased UV-light absorption capability of Fe/TiO_2 compared to pure titania; (b) inhibition of rutile phase formation due to a small amount of Fe; (c) acting as both h^+/e^- traps to reduce the recombination rate of those pairs during the photodegradation. The last factor seems to play a significant role in case of the obtained results.

During irradiation of Fe-modified TiO_2 the following events could take place [25,26,38]:

1. Charge-pair generation:

$$TiO_2 + h\nu \rightarrow h^+ + e^- \quad (24)$$

$$Fe^{3+} + h\nu \rightarrow Fe^{4+} + e^- \quad (25)$$

$$Fe^{3+} + h\nu \rightarrow Fe^{2+} + h^+ \quad (26)$$

2. Charge trapping

$$Ti^{4+} + e^- \rightarrow Ti^{3+} \quad (27)$$

$$Fe^{3+} + e^- \rightarrow Fe^{2+} \quad (28)$$

$$Fe^{3+} + h^+ \rightarrow Fe^{4+} \quad (29)$$

3. Charge release and migration

$$Fe^{2+} + Ti^{4+} \rightarrow Fe^{3+} + Ti^{3+} \quad (30)$$

4. Recombination

$$e^- + h^+ \rightarrow TiO_2 \quad (31)$$

$$Fe^{2+} + h^+ \rightarrow Fe^{3+} \quad (32)$$

$$Fe^{4+} + e^- \rightarrow Fe^{3+} \quad (33)$$

$$Fe^{4+} + Ti^{3+} \rightarrow Fe^{3+} + Ti^{4+} \quad (34)$$

According to Hung et al. [17] the reactions (32)–(34) take place when Fe ions concentration is high and they act as recombination centres. However, a small amount of Fe ions can act as a photogenerated h^+ or e^- trap and inhibit the hole–electron recombination (Eqs. (27)–(30)) [25,26].

From the obtained results (Figs. 4 and 5) it could be found that the highest effectiveness of CH_4 formation was in case of the sample containing 20 wt.% of Fe (A-Fe20Ac500). The good photocatalytic activity of this sample might be attributed to the presence of ilmenite phase (Fig. 1). $FeTiO_3$ has a good light absorbance and favourable photo-excited electron–hole separation and lifetime of those pairs [39]. Above 20 wt.% of Fe, the activity towards CH_4 formation decreased (A-Fe30Ac500). One reason for that could be an increase of recombination rate, which was discussed earlier. Another one could be coverage of TiO_2 particles with Fe_3O_4 (Fig. 4). When concentration of Fe precursor used for modification is too high titania surface becomes overloaded and its accessibility to CH_3COOH molecules is significantly reduced. This results in a decrease of the reaction efficiency. In order to confirm the supposition that the presence of high amount of Fe_3O_4 could be responsible for the observed low photoactivity of the A-Fe30Ac500, an additional experiment was conducted, in which the commercially available Fe_3O_4 was applied as the photocatalyst. It was found that the yields of CH_4 and CO_2 production in the presence of this iron oxide were very low. After 5 h of irradiation the amounts of methane and carbon dioxide were 0.21 and 0.27 mmol/mol CH_3COOH, respectively. After 27 h of the process the amounts of both, CH_4 and CO_2 were equal to each other and reached 0.67 mmol/mol CH_3COOH. The efficiency of CH_4 generation in the presence of the commercial Fe_3O_4 was significantly lower than that measured during the process performed with the least active TiO_2 P25 (1.39 mmol/mol CH_3COOH). The obtained results might lead to the conclusion that high coverage of TiO_2 particles with Fe_3O_4 has a detrimental effect on the photocatalytic activity of the catalyst in the photo-Kolbe reaction. And vice versa, Fe amount at the level of 10 wt.% was too low to improve the effectiveness of methane generation (A-Fe10Ac400, A-Fe10Ac500, A-Fe10Ac600). The observed decrease of photocatalytic activity of these samples could be associated with the presence of the mixed oxide $Fe_{1.66}Ti_{0.34}O_3$. It could be supposed that the low Fe loading was sufficient only to change the number of active sites and the type of surface groups of the photocatalyst or led to enhancement of surface recombination which resulted in a decrease of photocatalytic activity [16].

3.2.2. Hydrogen production from acetic acid

As was mentioned earlier, amongst the gaseous products of the process hydrogen was also detected. The photocatalytic evolution of hydrogen in the presence of sacrificial agents has been already described in the literature [14,33,40–46]. In general, when the reducing agent, or hole scavenger, such as alcohol [33,42,45,46] or organic acid [14,33] is present in the solution, the photogenerated holes react with the reducing agent. As a result the photocatalyst is enriched with electrons and H_2 evolution reaction is enhanced [47]:

$$2H^+ + 2e^- \rightarrow H_2 \quad (35)$$

From the mechanism proposed by Sakata et al. [14] it can be found that H_2 is produced from methanol and glycolic acid, which are formed from acetic acid (Eqs. (10), (18), (22), (36), and (37)):

$$CH_3COOH + 2^{\bullet}OH \rightarrow HOCH_2COOH + H_2O \quad (36)$$

$$HOCH_2COOH + H_2O \rightarrow 2CO_2 + 3H_2 \quad (37)$$

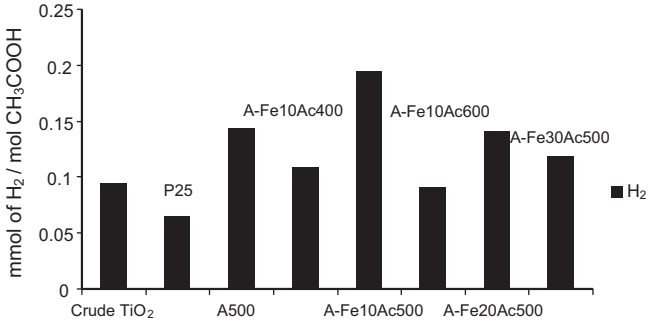

Fig. 6. Comparison of the amounts of H_2 evolved after 27 h of irradiation in the presence of different photocatalysts.

Patsoura et al. [33] reported that hydrogen was produced from different alcohols, organic acids and acetaldehyde, although in the presence of the latter compound rather low production rates were observed.

Fig. 6 shows H_2 concentration after 27 h of the irradiation. The highest yield of hydrogen evolution was observed for A-Fe10Ac500. After 5 h of the process the amount of H_2 was 0.04 mmol/mol CH_3COOH. A lengthening of the reaction time up to 27 h resulted in an increase of H_2 amount up to 0.19 mmol/mol CH_3COOH. The lowest efficiency of hydrogen formation was observed in case of P25 (0.06 mol/mol CH_3COOH at the end of experiment). The obtained results show that evolution of hydrogen was significantly lower than that of methane or carbon dioxide. The reason for that could be acidic pH of the reaction environment. It was reported that the H_2 production is favoured at neutral or basic solutions [33].

4. Conclusions

The gaseous products identified during the photocatalytic decomposition of CH_3COOH were CH_4, CO_2, C_2H_6, C_3H_8 and H_2. The concentrations of these compounds in the headspace volume of the reactor were dependent on the photocatalyst applied. Nevertheless, in all the experiments CH_4 and CO_2 were obtained at the highest amounts.

The most active photocatalyst toward CH_4 production was found to be A-Fe20Ac500 obtained by modification of crude TiO_2 with iron acetate (20 wt.% of Fe) and calcination at 500 °C in argon atmosphere. This sample contained primarily anatase (95%) with crystallite size of 24 nm. A good photocatalytic activity of this sample was attributed to the presence of ilmenite $FeTiO_3$.

Low effectiveness of CH_4 generation and very high yield of CO_2 formation in case of TiO_2 P25 was attributed to mineralization of acetic acid by photogenerated oxygen. The photocatalytic generation of O_2 was associated with high effectiveness of hydroxyl radicals formation in the presence of P25. Thus, it could be concluded that a high concentration of hydroxyl radicals is not desirable for methane formation from acetic acid under N_2 atmosphere.

In case of Fe/TiO_2 it was found that the effectiveness of hydrocarbons and hydrogen generation was influenced mainly by the amount of Fe. No clear influence of the specific BET surface area on the evolution rate of gaseous products was observed.

The results of the presented investigations show that photocatalytic decomposition of acetic acid could be regarded as a method of production of environmentally friendly "photo-biogas" containing useful hydrocarbons (CH_4, C_2H_6 and C_3H_8) and H_2. In the presented system after 27 h only the amount of methane was 3.36 mmol/mol CH_3COOH which corresponds to 6.93% of CH_4 in the gas phase when the head space volume of the reactor applied is taken into account. A lengthening of the irradiation time could lead to an increase of

methane concentration. However, since the efficiency of the presented system remains low, further investigations aiming at the design of efficient photocatalyst in order to improve the process performance are necessary. Moreover, an application of organic substrates other than acetic acid should be considered. These two key issues are the subject of further investigations.

Acknowledgement

This work has been supported by the Polish Ministry of Science and Higher Education as a scientific project N N523 413435 (2008–2011).

References

[1] S. Yadvika, T.R. Sreekrishnan, V. Kohli, A. Rana, Enhancement of biogas production from solid substrates using different techniques – a review, Bioresour. Technol. 95 (2004) 1–10.
[2] G. Lastella, C. Testa, G. Cornacchina, M. Notornicola, F. Voltasio, V.K. Sharma, Anaerobic digestion of semi-solid organic waste: biogas production and its purification, Energ. Convers. Manage. 43 (2002) 63–75.
[3] Y. Chen, J.J. Cheng, K.S. Creamer, Inhibition of anaerobic digestion process: a review, Bioresour. Technol. 99 (2008) 4044–4064.
[4] V. Augugliaro, M. Litter, L. Palmisano, J. Soria, The combination of heterogeneous photocatalysis with chemical and physical operations: a tool for improving the photoprocess performance, J. Photochem. Photobiol. C 7 (2006) 127–144.
[5] Y. Ku, W.H. Lee, W.Y. Wang, Photocatalytic reduction of carbonate in aqueous solution by UV/TiO_2 process, J. Mol. Catal. A: Chem. 212 (2004) 191–196.
[6] S.S. Tan, L. Zou, E. Hu, Photosynthesis of hydrogen and methane as key components for clean energy system, Sci. Tech. Adv. Mater. 8 (2007) 89–92.
[7] S.S. Tan, L. Zou, E. Hu, Photocatalytic reduction of carbon dioxide into gaseous hydrocarbon using TiO_2 pellets, Catal. Today 115 (2006) 269–273.
[8] M. Anpo, H. Yamashita, Y. Ichihashi, S. Ehara, Photocatalytic reduction of CO_2 with H_2O on various titanium oxide catalysts, J. Electroanal. Chem. 396 (1995) 21–26.
[9] K. Koči, L. Obalová, Z. Lacný, Photocatalytic reduction of CO_2 over TiO_2 based catalysts, Chem. Pap. 62 (2008) 1–9.
[10] M. Subrahmanyam, S. Kaneco, N. Alonso-Vante, A screening for the photo reduction of carbon dioxide supported on metal oxide catalysts for C_1–C_3 selectivity, Appl. Catal. B 23 (1990) 169–174.
[11] B. Kraeutler, A.J. Bard, Photoelectrosynthesis of ethane from acetate ion at an n-type TiO_2 electrode. The photo-Kolbe reaction, J. Am. Chem. Soc. 99 (1977) 7729–7731.
[12] B. Kraeutler, A.J. Bard, Heterogenous photocatalytic synthesis of methane from acetic acid – new Kolbe reaction pathway, J. Am. Chem. Soc. 100 (1978) 2239–2240.
[13] B. Kraeutler, C.D. Jaeger, A.J. Bard, Direct observation of radical intermediates in the photo-Kolbe reaction – heterogenous photocatalytic radical formation by Electron Spin Resonance, J. Am. Chem. Soc. 100 (1978) 4903–4905.
[14] T. Sakata, T. Kawai, K. Hashimoto, Heterogenous photocatalytic reactions of organic acids in water. New reaction paths besides the photo-Kolbe reaction, J. Phys. Chem. 88 (1984) 2344–2350.
[15] G.R. Dey, K.K. Pushpa, Methane generated during photocatalytic redox reaction of alcohols on TiO_2 suspension in aqueous solutions, Res. Chem. Intermed. 32 (2006) 725–736.
[16] M. Zhou, J. Yu, B. Cheng, Effects of Fe-doping on the photocatalytic activity of mesoporous TiO_2 powders prepared by an ultrasonic method, J. Hazard. Mater. B 137 (2006) 1838–1847.
[17] W.C. Hung, Y.C. Chen, H. Chu, T.K. Tseng, Synthesis and characterization of TiO_2 and Fe/TiO_2 nanoparticles and their performance for photocatalytic degradation of 1,2-dichloroethane, Appl. Surf. Sci. 255 (2008) 2205–2213.
[18] M.A. Khan, S.I. Woo, O.B. Yang, Hydrothermally stabilized Fe(III) doped titania active under visible light for water splitting reaction, Int. J. Hydrogen Energy 33 (2008) 5345–5351.
[19] M.I. Litter, J.A. Navío, Photocatalytic properties of iron-doped titania semiconductors, J. Photochem. Photobiol. A 98 (1996) 171–181.
[20] K.T. Ranjit, B. Viswanathan, Synthesis, characterization and photocatalytic properties of iron-doped TiO_2, J. Photochem. Photobiol. A 108 (1997) 79–84.
[21] W.S. Tung, W.A. Daoud, New approach toward nanosized ferrous ferric oxide and Fe_3O_4-doped titanium dioxide photocatalysts, ACS Appl. Mater. Interface 1 (2009) 2453–2461.
[22] S. Zhu, Y. Li, C. Fan, D. Hang, W. Liu, Z. Dun, S. Wei, Structural studies of iron-doped TiO_2 nano-composites by Mossbauer spectroscopy, X-ray diffraction and transmission microscopy, Physica B 364 (2005) 199–205.
[23] Y.R. Smith, K.J.A. Raj, V. Subramanian, B. Viswanathan, Sulfated Fe_2O_3–TiO_2 synthesized from ilmenite ore: a visible light active photocatalyst, Colloid Surf. A: Physicochem. Eng. Aspects 367 (2010) 140–147, doi:10.1016/j.colsurfa.2010.07.001.
[24] G. Colón, J.M. Sánchez-España, M.C. Hidalgo, J.A. Navío, Effect of TiO_2 acidic pre-treatment on the photocatalytic properties for phenol degradation, J. Photochem. Photobiol. A 179 (2006) 20–27.
[25] K. Demeestere, J. Dewulf, T. Ohno, P. Herrera Salgado, H. Van Langenhove, Visible light mediated photocatalytic degradation of gaseous trichloroethylene and dimethyl sulfide on modified titanium dioxide, Appl. Catal. B 61 (2005) 140–149.
[26] M.H. Zhou, J.G. Yu, B. Cheng, H.G. Yu, Preparation photocatalytic activity of Fe-doped mesoporous titanium dioxide nanocrystalline photocatalysts, Mater. Chem. Phys. 93 (2005) 159–163.
[27] K. Ishibashi, A. Fujishima, T. Watanabe, K. Hashimoto, Detection of active oxidative species in TiO_2 photocatalysis using the fluorescence technique, Electrochem. Commun. 2 (2000) 207–210.
[28] J. Zhu, W. Zheng, B. Hea, J. Zhang, M. Anpo, Characterization of Fe–TiO_2 photocatalysts synthesized by hydrothermal method and their photocatalytic reactivity for photodegradation of XRG dye diluted in water, J. Mol. Catal. A 216 (2004) 35–43.
[29] Z. Ambrus, N. Balázs, T. Alapi, G. Wittmann, P. Sipos, A. Dombi, K. Mogyorósi, Synthesis, structure and photocatalytic properties of Fe(III)-doped TiO_2 prepared from $TiCl_3$, Appl. Catal. B 81 (2008) 27–37.
[30] H. Yoneyama, Y. Takao, H. Tamura, A.J. Bard, Factors influencing product distribution in photocatalytic decomposition of aqueous acetic acid on platinized TiO_2, J. Phys. Chem. 87 (1983) 1417–1422.
[31] D. Muggli, J.L. Falconer, Parallel pathways for photocatalytic decomposition of acetic acid on TiO_2, J. Catal. 187 (1999) 230–237.
[32] Y. Honghui, Y. Chen, L. Guo, Homogenous photocatalytic decomposition of acetic acid using UV-Fe^{2+}/Fe^{3+} system in the absence of oxygen, Catal. Commun. 11 (2010) 1099–1103.
[33] A. Patsoura, D.I. Kondarides, X.E. Verykios, Photocatalytic degradation of organic pollutants with simultaneous production of hydrogen, Catal. Today 124 (2007) 94–102.
[34] I.K. Konstantinou, T.A. Albanis, TiO_2-assisted photocatalytic degradation of azo dyes in aqueous solution: kinetic and mechanistic investigation. A review, Appl. Catal. B 49 (2004) 1–14.
[35] Z. Liu, X. Zhang, S. Nishimoto, T. Murakami, A. Fujishima, Efficient photocatalytic degradation of gaseous acetaldehyde by highly ordered TiO_2 nanotube arrays, Environ. Sci. Technol. 42 (2008) 8547–8551.
[36] I. Sopyan, M. Watanabe, S. Murasawa, K. Hashimoto, A. Fujishima, An efficient TiO_2 thin-film photocatalyst: photocatalytic properties in gas-phase acetaldehyde degradation, J. Photochem. Photobiol. A 98 (1996) 79–86.
[37] I.H. Tseng, W.Ch. Chang, J.C.S. Wu, Photoreduction of CO_2 using sol–gel derived titania and titania-supported copper catalysts, Appl. Catal. B 37 (2002) 37–48.
[38] C.Y. Wang, C. Böttcher, D.W. Bahnemann, J.K. Dohrmann, A comparative study of nanometer sized Fe(III)-doped TiO_2 photocatalysts: synthesis, characterization and activity, J. Mater. Chem. 13 (2003) 2322–2329.
[39] F.X. Ye, T. Tsumura, K. Nakata, A. Ohmoric, Dependence of photocatalytic activity on the compositions and photo-absorption of functional TiO_2–Fe_3O_4 coatings deposited by plasma spray, Mater. Sci. Eng. B 148 (2008) 154–161.
[40] K.G. Kanade, B.B. Kale, J.O. Baeg, S.M. Lee, Ch.W. Lee, S.J. Moon, H. Chang, Self-assembled aligned Cu doped ZnO nanoparticles for photocatalytic hydrogen production under visible light irradiation, Mater. Chem. Phys. 102 (2007) 98–104.
[41] J.S. Jang, H.G. Kim, P.H. Borse, J.S. Lee, Simultaneous hydrogen production and decomposition of H_2S dissolved in alkaline water over CdS–TiO_2 composite photocatalysts under visible light irradiation, Int. J. Hydrogen Energy 32 (2007) 4786–4791.
[42] A. Kudo, Y. Miseki, Heterogeneous photocatalyst materials for water splitting, Chem. Soc. Rev. 38 (2009) 253–278.
[43] Z. Zou, H. Arakawa, Direct water splitting into H_2 and O_2 under visible light irradiation with a new series of mixed oxide semiconductor photocatalysts, J. Photochem. Photobiol. A 158 (2003) 145–162.
[44] Z. Jin, X. Zhang, Y. Li, S. Li, G. Lu, 5.1% Apparent quantum efficiency for stable hydrogen generation over eosin-sensitized CuO/TiO_2 photocatalyst under visible light irradiation, Catal. Commun. 8 (2007) 1267–1273.
[45] H.J. Choi, M. Kang, Hydrogen production from methanol/water decomposition in a liquid photosystem using the anatase structure of Cu loaded TiO_2, Int. J. Hydrogen Energy 32 (2007) 3841–3848.
[46] J. Bandara, C.P.K. Udawatta, C.S.K. Rajapakse, Highly stable CuO incorporated TiO_2 catalyst for photocatalytic hydrogen production from H_2O, Photochem. Photobiol. Sci. 4 (2005) 857–861.
[47] N. Sasirekha, S.J.S. Basha, K. Shanthi, Photocatalytic performance of Ru doped anatase mounted on silica for reduction of carbon dioxide, Appl. Catal. B 62 (2006) 169–180.